

# Point Cloud Oversegmentation with Graph-Structured Deep Metric Learning

Loic Landrieu<sup>1</sup>, Mohamed Boussaha<sup>2</sup>

Univ. Paris-Est, IGN-ENSG, LaSTIG, <sup>1</sup>STRUDEL, <sup>2</sup>ACTE, Saint-Mandé, France

loic.landrieu@ign.fr, mohamed.boussaha@ign.fr

## Abstract

We propose a new supervised learning framework for oversegmenting 3D point clouds into superpoints. We cast this problem as learning deep embeddings of the local geometry and radiometry of 3D points, such that the border of objects presents high contrasts. The embeddings are computed using a lightweight neural network operating on the points' local neighborhood. Finally, we formulate point cloud oversegmentation as a graph partition problem with respect to the learned embeddings.

This new approach allows us to set a new state-of-the-art in point cloud oversegmentation by a significant margin, on a dense indoor dataset (S3DIS) and a sparse outdoor one (vKITTI). Our best solution requires over five times fewer superpoints to reach similar performance than previously published methods on S3DIS. Furthermore, we show that our framework can be used to improve superpoint-based semantic segmentation algorithms, setting a new state-of-the-art for this task as well.

## 1. Introduction

The interest of segmenting point clouds into sets of points known as superpoints—the 3D equivalent of superpixels—as a preprocessing step to their analysis has been extensively demonstrated [32, 44, 40, 7, 56]. However, these unsupervised methods rely on the assumption that segments which are geometrically and/or radiometrically homogeneous are also semantically homogeneous. This assertion should be challenged, especially since the quality of any further analysis is limited by the quality of the initial oversegmentation. Our objective in this paper is to formulate a supervised framework for oversegmenting 3D point clouds into semantically pure superpoints in order to facilitate their semantic segmentation.

Although superpixel-based methods and deep learning have both been around for a long time in computer vision, convolutional neural networks have only recently been used for superpixel oversegmentation. Notably, [37] introduced a loss function emulating oversegmentation metrics, and

which is compatible with graph-based clustering methods. [28] propose a fully differentiable version of the SLIC superpixel algorithm [1], allowing for end-to-end training of spatial clustering methods. Both approaches have shown promising results, displaying significant improvement upon methods relying on handcrafted descriptors. In this paper, we build upon these ideas, albeit in the 3D setting.

We propose formulating point cloud oversegmentation as a deep metric learning problem structured by an adjacency graph defined on an input 3D point cloud. We introduce the *graph-structured contrastive loss*, a loss function which learns to embed 3D points homogeneously within objects and with high contrast at their interface. This loss can be adapted to the non-differentiable task of oversegmentation by using our *cross-partition weighting* strategy. The points' embeddings themselves are computed from the points' local geometry and radiometry by a lightweight model inspired from PointNet [41] and called *Local Point Embedder* (LPE). Finally, the superpoints are defined as a piecewise-constant approximation of the learned embedding in the adjacency graph, in the manner of [21].

Furthermore, we define the end-goal of our point cloud oversegmentation as assisting semantic segmentation methods by providing semantically pure superpoints. We show that our approach can be integrated with the superpoint graph approach of [32] to significantly improve the partition step, and consequently the resulting semantic segmentation. The contributions of this paper are as follows:

- We present the first supervised framework for 3D point cloud oversegmentation;
- We introduce the graph-structured contrastive loss, which can be combined with our cross-partition weighting strategy to produce point embeddings with high contrast at objects' borders;
- We introduce the local point embedder, a lightweight architecture, inspired by [41], to embed the local geometry and radiometry of 3D points in a compact way;
- We significantly improve the state-of-the-art of point cloud oversegmentation for two well-known and very different datasets;

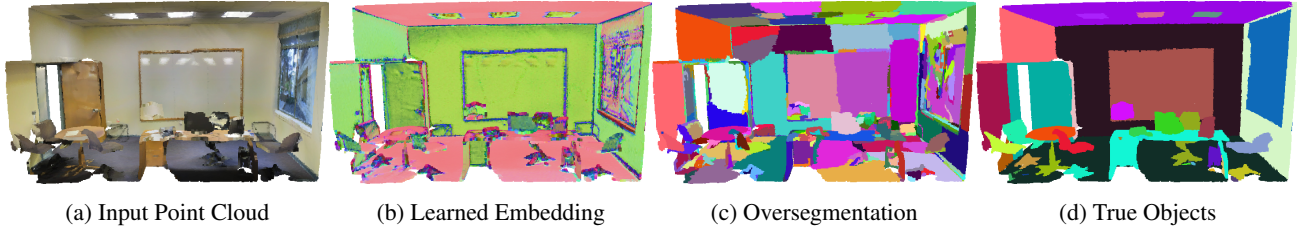


Figure 1: Illustration of our framework on a hard-to-segment scene with a white board on a white wall: a colored point cloud is given as input (a), an embedding is computed for each point (b), which allows a clustering technique to compute an oversegmentation (c), which closely follows the ground truth (d). Throughout the figures of this paper, the embeddings are projected into a 3-dimensional space to allow color visualization.

- When combined with the superpoint graph semantic segmentation method, our approach improves upon the state-of-the-art for this task as well.

## 2. Related work

**Superpixels/ Supervoxels:** There is a large body of literature on the oversegmentation of images into superpixels [49] and videos into supervoxels [57]. These methods can be divided into two groups: graph-based, which exploit the pixels’ connectivity [14, 20, 36], and cluster-based, which use the pixels’ relative positions [1, 51, 58, 33]. Recently, deep learning methods have been successfully used to develop supervised superpixels oversegmentation approaches, either graph-based [37], or cluster-based [28].

**Oversegmentation of 3D Point Clouds:** The aforementioned methods perform well on images, but rely on the regular structure of pixels. 3D point clouds, as unordered point sets with irregular distributions, require special attention. [4] propose three extensions of 2D local variation graph-based method [14] to 3D oversegmentation and study different strategies for constructing the graph, edge weights, and subgraph merging. [48] introduce a graph-structured approach which exploits the structure of LiDAR sensors to remove edges corresponding to boundary points. [39] propose a cluster-based method based on the  $k$ -means algorithm and octrees. However, this method remains sensitive to the clusters’ initialization. [15] use the visual saliency of RGBD images to initialize clustering. [35] propose a clustering method which does not require such initialization, and is therefore less sensitive to the irregular densities of LiDAR point clouds. Likewise, [21] introduce an initialization-free segmentation model formulated as a graph-structured optimization problem. All these methods rely on hand-crafted geometric and/or colorimetric features.

**Deep Learning for 3D Point Clouds:** The work in [41] has pioneered the use of deep learning for 3D point cloud processing. However, this usage has so far only been used for semantic segmentation [34, 50, 10, 46, 43, 42, 59, 54], object detection [62], or reconstruction [19]. To the best of

our knowledge, no supervised 3D point oversegmentation technique that leverages deep learning-based embeddings to generate superpoints has been developed yet.

**Metric Learning:** Metric learning aims to learn a similarity function between data points with properties corresponding to a given task [30]. In practice, an embedding function associates each data point with a feature vector attuned to a given objective. These objectives can be related to classification [16, 45], or clustering [47, 23], among many other applications (see [2] for a useful taxonomy). In the context of deep learning, this can be achieved by using a well-chosen loss, such as the contrastive loss [8, 5]; the triplet loss [24] or some of its variants [53]. Notably, metric learning has recently been used to improve the quality of learned features for a 3D point semantic segmentation task [12]. However, our task is different in the sense that our embeddings are related to oversegmentation through a graph partition problem rather than classification.

## 3. Method

Our goal is to produce a high-quality 3D-point cloud oversegmentation, so that it can be in turn used by superpoint-based semantic segmentation algorithms. This translates into the following three properties:

- (P1) **object-purity:** superpoints must not overlap over objects, especially if their semantics are different;
- (P2) **border recall:** the interface between superpoints must coincide with the borders between objects;
- (P3) **regularity:** the shape and contours of the superpoints must be simple.

Our approach can be broken down into two steps: in Section 3.1 we present the local cloud embedder, a simple neural network which associates each point with a compact embedding that captures its local geometry and radiometry. In Section 3.2, we describe how we compute a point cloud oversegmentation from this embedding using either graph or cluster-based oversegmentation algorithms.

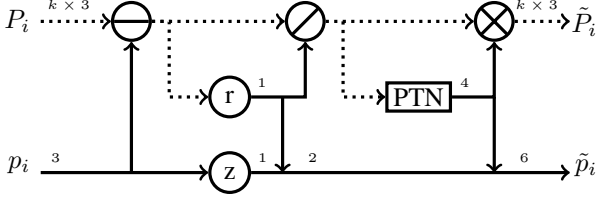


Figure 2: Architecture of the spatial transform network. It takes a point’s coordinate as point-input  $p_i$  and the coordinates of its neighbors as set-input  $P_i$ . The vertex  $r$  computes the radius of a point cloud (1), the vertex  $z$  extract the vertical coordinate of a point’s position, and the vertex PTN is a small PointNet-like network (2) which outputs a  $2 \times 2$  rotation matrix around the  $z$  axis (4). In this and subsequent figures, set-features (respectively point-features) are represented by a dotted line (respectively a solid line). The numbers above the lines represent the size of the channels.

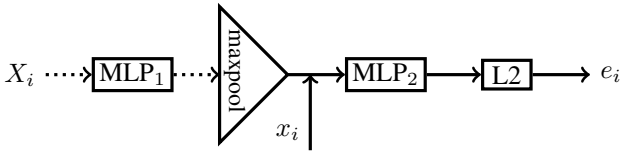


Figure 3: Architecture of the local point embedder (LPE) (7), which computes an embedding set-feature  $X_i$  and point-feature  $x_i$  encoding the local radiometry and the normalized geometry. The  $L_2$  block normalizes the output on the unit sphere (6).

Throughout this paper we will stress the difference between *set-features*, which are unordered sets of descriptors (such as information related to the neighbors of a point), and *point-features*, which characterize a specific point. Set features will always be capitalized, while point-features will use lowercase.

Let us consider a point cloud  $C$ , with each point  $i$  defined with its position  $p_i \in \mathbb{R}^3$  and  $d$ -dimensional radiometric information  $r_i \in \mathbb{R}^d$  (this can be colors if available, or intensity for LiDAR scans, or be ignored if none is available). Each point  $i$  is associated with the set-features  $P_i$  and  $R_i$ , respectively comprised of the position and radiometry of its  $k$  nearest neighbors  $N_i$  in the input cloud:  $P_i = \{p_j \mid j \in N_i\}$ ,  $R_i = \{r_j \mid j \in N_i\}$ . For ease of notation, any operator or function  $f$  applied to a set-feature  $X$  is to be understood as being applied to all its elements:  $f(X) = \{f(x) \mid x \in X\}$ .

### 3.1. Local Point Embedding

Our objective is to associate to each point a compact  $m$ -dimensional embedding  $e_i$  characterizing its point-features (position, color, etc.) and the geometry and radiometry of its local neighborhood. The embeddings are constrained to be within the  $m$ -unit sphere  $\mathbb{S}_m$ , as suggested by [52], to

prevent collapse during the training phase, and to normalize their distance with one another.

To this end, we introduce the Local Point Embedder (LPE), a lightweight network inspired by PointNet [41]. However, unlike PointNet, LPE does not try to extract information from the whole input point cloud, but rather encodes each point based on purely local information. Here, we describe the different units of our network.

**Spatial Transform:** This unit takes the positions of a target point  $p_i$  and its local  $k$ -neighborhood  $P_i$ , as represented in Figure 2. It normalizes the neighbors’ coordinates around  $p_i$ , and such that the standard deviation of the point’s position is equal to 1 (3). Then, this neighborhood is rotated around the  $z$  axis with a  $2 \times 2$  rotation matrix computed by small PointNet network PTN (4). As advocated by [27], these steps aim to standardize the position of the neighborhood clouds of each point. This helps the next network to learn position distribution. Along the normalized neighborhood position  $\tilde{P}_i$ , this unit also outputs geometric point-features  $\tilde{p}_i$  describing the elevation  $p_i^{(z)}$ , the neighborhood radius, as well as its original orientation (through the 4 values of the rotation matrix:  $[\Omega_{x,x}, \Omega_{x,y}, \Omega_{y,x}, \Omega_{y,y}]$ ) (5). By keeping track of the normalization operations, the embedding can stay covariant with the original neighborhood’s radius, height, and original orientation, even though the points’ positions have been normalized and rotated.

$$(1) \text{ rad} = \text{std}(P_i) \quad \tilde{P}_i = \{p \times \Omega \mid p \in P_i'\} \quad (4)$$

$$(2) \Omega = \text{PTN}(\tilde{P}_i) \quad \tilde{p}_i = [p_i^{(z)}, \text{rad}, \Omega] \quad (5)$$

$$(3) P_i' = (P_i - p_i)/\text{rad}$$

**Local Point Embedder:** The LPE network, represented in Figure 3, computes a normalized embedding from two inputs: a point-feature  $x_i$  and a set-feature  $X_i$ . As in PointNet [41], the set-features are first processed independently by a multi-layer perceptron (denoted  $\text{MLP}_1$ ) comprised of a succession of layers in the following order: linear, activation (ReLU [38]), normalization (batch [26]), and so on. The resulting set-features are then maxpooled into a point-feature, which is concatenated with the input point-feature. The resulting vector is processed through another multi-layer perceptron  $\text{MLP}_2$  (7), and finally normalized on the unit sphere.

The embeddings  $e_i$  are computed for each point  $i$  of  $C$  through a shared LPE (8). The input set-feature  $X_i$  is set as the concatenation of the neighbour’s transformed position  $\tilde{P}_i$  and their radiometric information  $R_i$ , while the input point-feature  $x_i$  is composed of the neighborhood geometric point-feature  $\tilde{p}_i$  and the radiometry  $r_i$  of point  $i$ .

$$L_2(\cdot) = \cdot / \|\cdot\| \quad (6)$$

$$\text{LPE}(X_i, x_i) = L_2(\text{MLP}_2([\max(\text{MLP}_1(X_i)), x_i])) \quad (7)$$

$$e_i = \text{LPE}([\tilde{P}_i, R_i], [\tilde{p}_i, r_i]) \quad (8)$$

## 3.2. Graph-Based Point Cloud Oversegmentation

### 3.2.1 The Generalized Minimal Partition Problem

Once the embeddings are computed, we define the superpoints with respect to an adjacency graph  $G = (C, E)$  derived from the point cloud  $C$ . Note that  $E$  can be obtained from the neighbors' structure used for the LPE. However, we find that much smaller neighborhoods are needed to capture the cloud's adjacency structure than to describe the local neighborhood of points. As proposed by [21], we define the superpoints as the constant connected components in  $G$  of a piecewise-constant approximation of the embeddings  $e \in \mathbb{S}_m^C$ . This approximation is the solution  $f^*$  of the following optimization problem:

$$f^* = \arg \min_{f \in \mathbb{R}^{C \times m}} \sum_{i \in C} \|f_i - e_i\|^2 + \sum_{(i,j) \in E} w_{i,j} [f_i \neq f_j], \quad (9)$$

with  $w \in \mathbb{R}_+^E$  the edges' weight and  $[x \neq y]$  equal to 0 if  $x = y$  and 1 otherwise. To encourage the network to split along high contrast areas, we define the edge weight as  $w_{i,j} = \lambda \exp\left(\frac{-1}{\sigma} \|e_i - e_j\|^2\right)$ , with parameters  $\lambda, \sigma \in \mathbb{R}^+$ .

Problem (9), known as the *generalized minimal partition* (GMP) and introduced by [31], is neither continuous, differentiable, nor convex, and therefore the global minimum cannot be realistically retrieved. However, the  $\ell_0$ -cut pursuit algorithm [31] allows for fast approximate solutions.

The contour penalty automatically implements (P3) for reasonable parameterization of the problem. Note that the optimization variable  $f$  can take its values in  $\mathbb{R}^{C \times m}$ , while each embedding  $e_i$  is constrained on the  $m$ -sphere. This is a limitation of our approach due to efficiency concerns. It can lead to some suboptimal approximate solutions. However, we show in the numerical experiments that the learned embeddings lead to satisfactory partitions.

### 3.2.2 Graph-Structured Contrastive Loss

As mentioned earlier, the semantic purity property (P1) is the first quality of superpoints. One could imagine taking a metric estimating the semantic purity of the solution of (9) as a loss function. However, the GMP is a non-continuous non-convex optimization problem, and computing connected components on a graph is inherently non-differentiable. This makes optimizing directly with respect to properties of the partition very hard, if not impossible.

Instead, we note that if the border recall property (P2) is implemented (*i.e.* superpoints and objects share the same boundaries), then (P1) ensues. Therefore, we propose a surrogate loss called *graph-structured contrastive loss* focusing on correctly detecting the borders between objects. To this end, we define  $E_{\text{intra}}$  (resp.  $E_{\text{inter}}$ ) the set of *intra-edges* (resp. *inter-edges*) as the set of edges of  $G$  between

points within the same object (resp. point from different adjacent objects).

In the spirit of the original contrastive loss [8], our loss encourages embeddings of vertices linked by an intra-edge to be similar, while rewarding different embeddings when linked by an inter-edge:

$$\ell(e) = \frac{1}{|E|} \left( \sum_{(i,j) \in E_{\text{intra}}} \phi(e_i - e_j) + \sum_{(i,j) \in E_{\text{inter}}} \mu_{i,j} \psi(e_i - e_j) \right),$$

with  $\phi$  (resp.  $\psi$ ) a function minimal (resp. maximal) at 0, and  $\mu_{i,j} \in \mathbb{R}^{E_{\text{inter}}}$  a weight on inter-edges. A point embedding function minimizing this loss will be uniform within objects and have stark contrasts at their interface. Consequently, the components of the piece-wise constant approximation of (9) should follow the objects' borders. This loss differs from the triplet loss [24, 52], as it involves all vertices within a graph (or a sub-graph) at once, and not just an anchor and related positive/negative examples. In this way, it bypasses the problem of example picking altogether. Indeed, the positive and negative examples are directly given by the adjacency structure set by  $E_{\text{intra}}$  and  $E_{\text{inter}}$ . It differs from [12] as it does not try to learn semantic information, but rather to compute a signal on a graph such that its constant approximation respects certain properties, with no attention to semantics. Indeed, objects of different classes can share the same embeddings as long as they are never adjacent, such as floors and ceilings for indoor scenes.

We chose  $\phi$ , the function promoting intra-object homogeneity as  $\phi(x) = \delta(\sqrt{\|x\|^2/\delta^2 + 1} - 1)$  with  $\delta = 0.3$  (represented in Figure 4). This means that the first term of  $\ell$  is the (pseudo)-Huber graph-total variation on the  $E_{\text{intra}}$  edge [25, 6], promoting smooth homogeneity of embeddings within the same object.

With  $\psi(x) = \max(1 - \|x\|, 0)$ , the second part of  $\ell$  is the opposite of the truncated graph-total variation [61] on the inter-edges. It penalizes similar embeddings at the border between objects. Conscious that our embeddings are restricted to the unit sphere, we threshold this function for differences larger than 1 (corresponding to a 60 degree angle). In other words,  $\psi(x)$  encourages vertices linked by an inter-edge to take embeddings with an euclidean distance of 1, but does not push for a larger difference.

Note that any embeddings that are constant within ob-

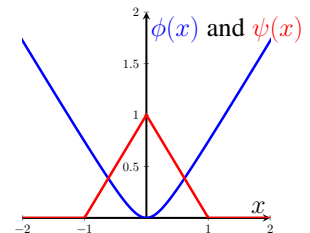


Figure 4: The functions  $\phi$  (in blue) and  $\psi$  (in red) used in the graph-structured contrastive loss.

jects, and with a difference of at least 1 between adjacent objects, will have 0 loss. The four-color theorem [17] tells us that it is always possible as long as the dimension of our embedding is at least 3. However, because embeddings are computed by the LPE, borders which do not present recognizable geometric or radiometric configurations cannot be recovered by our method.

### 3.2.3 Cross-Partition Weighting

The choice of  $\mu_{i,j}$  plays a crucial role in the efficiency of the graph-structured contrastive loss. Although (P2) does imply (P1), small errors in the former can have drastic consequences in the latter. Indeed, a single missed edge can erroneously fuse two large superpoints covering different objects. Therefore, we need to incorporate the induced partition’s purity into the loss.

[37] introduced the segmentation-aware affinity loss (SEAL) implementing this idea. They propose weighting intra-edges as 1, and inter-edges as  $\mu_{i,j} = 1 + |S| - |S \setminus O_S|$  for  $i$  and  $j$  within the same superpoint  $S$ , with  $O_S$  the majority-object, i.e. the object for which most points of  $S$  belongs to. Although [37] boasts impressive results for superpixel oversegmentation, we were not able to extend this success within our framework. We believe this stems from three reasons: (i) all border edges of a superpoint are weighted identically regardless of their influence on the purity and the size of the interface; (ii) as soon as a superpoint no longer overlaps an object’s border, its weight decreases dramatically to 1, making the loss very unstable; (iii) [37] uses a different graph-based clustering[36].

To overcome these limitations, we introduce the cross-partition weighting strategy. We first compute the *cross-segmentation graph*  $\mathcal{G} = (\mathcal{C}, \mathcal{E})$ , defined as the adjacency graph of the cross-partition  $\mathcal{C}$  of  $\mathcal{C}$  between the superpoints partition  $\mathcal{S}$  and the object partition  $\mathcal{O}$ . In other words,  $\mathcal{C}$  is the set of connected components of the graph  $G$  when all edges either between objects *or* between superpoints are removed, and the *super-edge* (i.e. set of edges)  $(U, V) \in \mathcal{E}$  is the set of inter-edges of  $E_{\text{inter}}$  between  $U$  and  $V$  in  $\mathcal{C}$ :

$$\begin{aligned} \mathcal{C} &= \{O \cap S \mid O \in \mathcal{O}, S \in \mathcal{S}\} \\ \mathcal{E} &= \{(i, j) \in (U \times V) \cap E_{\text{inter}} \mid U, V \in \mathcal{C}\}. \end{aligned}$$

We associate the following weight  $\mu_{U,V}$  to each superedge  $(U, V)$  and  $\mu_{i,j}$  to each edge:

$$\begin{aligned} \mu_{U,V} &= \frac{\mu \min(|U|, |V|)}{|(U, V)|} && \text{for } (U, V) \in \mathcal{E} \\ \mu_{i,j} &= \mu_{U,V} && \text{for all } (i, j) \in (U, V) \end{aligned}$$

with  $\mu$  a parameter of the model. Such weights simultaneously take into account the influence of the edges in the purity and the shape of the interfaces. Indeed, should an

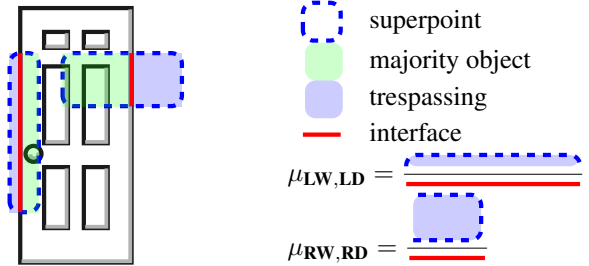


Figure 5: Illustration of the cross-partition weighting strategy on a scene comprised of a door (D) and a wall (W). Two superpoints L (left) and R (right) overlap the door. The superedge (LW, LD) (resp. (RW, RD)) represent the adjacency between the part of the left (resp. right) superpoint covering the wall and the part covering the door. With fewer trespassing points and a longer interface than (RW, RD), the weights of the edges constituting (LW, LD) are smaller.

edge of the superedge  $(U, V)$  be missed as a border, the superpoints  $U$  and  $V$  would be merged. Since  $U$  and  $V$  cover different objects (by definition of  $\mathcal{E}$ ), such a merger would induce at least  $\min(|U|, |V|)$  vertices *trespassing*, i.e. not being in the majority-object of the merged superpoint. The weights are also divided by the number of edges constituting the interface between  $U$  and  $V$  in order to distribute evenly the penalty over the number of edges constituting an interface. This prevents long borders from being over-represented in the loss. See Figure 5 for an illustration.

### 3.3. Cluster-Based Oversegmentation

We also implemented a generalization of the method of [28] to the 3D setting. The main advantage of this approach is that the loss can directly implement (P1) through the cross-entropy of the averaged semantic classes within superpoints. However, this approach remains hindered by its sensitivity to the superpoint initialization, and its inability to adapt the superpoints’ size to the local complexity of the scene. Furthermore, as it bypasses (P3), it produces superpoints with complicated contour.

### 3.4. Implementation Details

We use a modified version of the  $\ell_0$ -cut pursuit algorithm<sup>1</sup>[31], with two main differences:

- to prevent the creation of many small superpoints in regions of high contrast, we merge components greedily with respect to the objective energy defined in (9), as long as they are smaller than a given threshold ;
- we heuristically improved the forward step (8) from [31], such that the regularization strength increases geometrically by a factor (of 0.7) along the iterations.

<sup>1</sup><https://github.com/loicland/cut-pursuit>

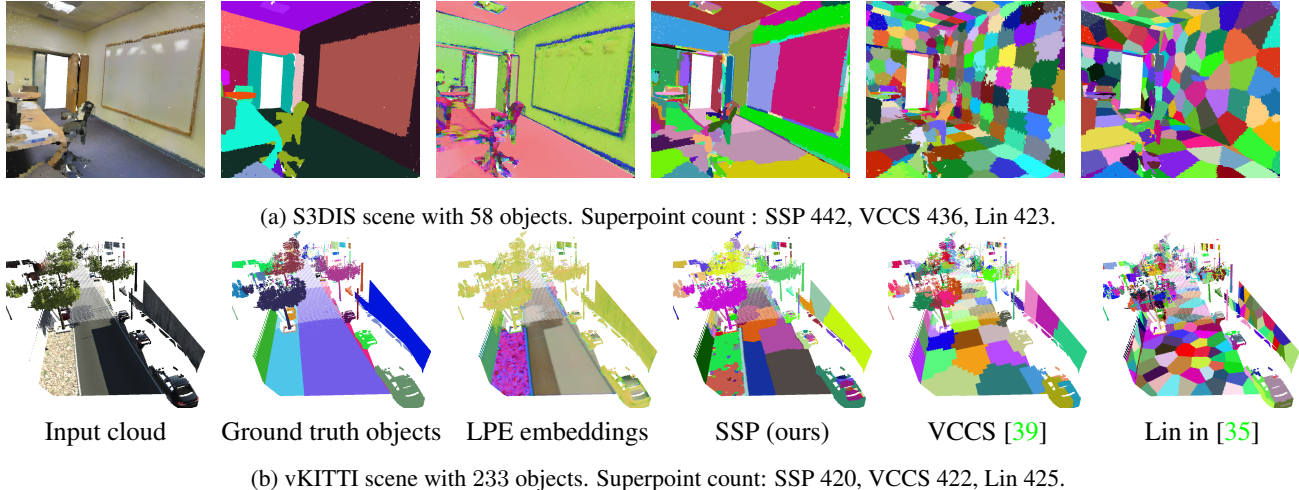


Figure 6: Illustration of the oversegmentations of our framework, and from competing algorithms.

This helps improve the quality of the lower optima retrieved, and consequently the oversegmentation’s.

To limit the size of the superpoints we concatenate to the points’ embeddings their 3D coordinates in (9) multiplied by a parameter  $\alpha_{\text{spatial}}$ , in the manner of [1]. This determines the maximum size that superpoints can reach.

In all our experiments, we set  $m$  the dimension of our embeddings to 4. We choose a light architecture for the LPE, with less than 15, 000 parameters. The exact network configurations for each dataset are detailed in the appendix.

## 4. Numerical Experiments

### 4.1. Datasets

We evaluate our approach on two datasets of different natures. The first one is S3DIS [3], composed of dense indoor scans of rooms in an office setting. The second one is vKITTI [10], an outdoor dataset of urban scenes that mimics sparse LiDAR acquisitions. Note that only S3DIS has individual object annotation. We consider the objects of vKITTI to be the connected components of the semantic labels in the adjacency graph  $G$ . For vKITTI, we consider the performance of our algorithm with and without color information. Both datasets are large scale (close to 600 million points for S3DIS and close to 15 million for vKITTI). We subsample them using a regular grid of voxels (3cm wide for S3DIS and 5cm wide for vKITTI). In each voxel, we average the position and color of the contained points. This allows us to decrease the computation time and memory load.

### 4.2. Point Cloud Oversegmentation

**Evaluation Metrics:** There are many standard metrics which assess the quality of point cloud oversegmentations with respect to properties (P1), (P2), and (P3). In particular, the Boundary Recall (BR) and Precision (BP) are used

to evaluate the ability of the superpoints to adhere to, and not cross, object boundaries ((P2), (P3)). In the literature, these measures are defined with respect to *boundary pixels* [39] or points [35]. However, we argue that transition occurs *between* points and not *at* points for point clouds. Consequently, we define  $E_{\text{inter}}^{\text{pred}}$  the set of predicted transition, *i.e.* the subset of edges of  $E$  that connect two points of  $C$  in two different superpoints. These metrics are often given with respect to a tolerance, *i.e.* the distance at which a predicted transition must take place from an actual object’s border for the latter to be considered retrieved. We set this distance to 1 edge, which leads us to define  $E_{\text{inter}}^{(1)}$  the set of inter-edges expanded to all directly adjacent edges in  $E$ :

$$E_{\text{inter}}^{(1)} = \{(i, j) \in E \mid \exists (i, k) \text{ or } (j, k) \in E_{\text{inter}}\}.$$

This allows us to define the boundary recall and precision with 1 edge tolerance for a set of predicted transition  $E_{\text{inter}}^{\text{pred}}$ :

$$BR = \frac{|E_{\text{inter}}^{\text{pred}} \cap E_{\text{inter}}^{(1)}|}{|E_{\text{inter}}^{\text{pred}}|}, \quad BP = \frac{|E_{\text{inter}}^{\text{pred}} \cap E_{\text{inter}}^{(1)}|}{|E_{\text{inter}}^{(1)}|}.$$

Since the end-goal of our point cloud oversegmentation framework is to provide useful superpoints for semantic segmentation, we define the *Oracle Overall Accuracy* (OOA). To assess object purity (P1), this metric characterizes the accuracy of the labeling that associates each superpoint  $S$  of a segmentation  $\mathcal{S}$  with its majority ground-truth label. Formally, let  $l \in \mathcal{K}^C$  be the semantic labels of each point within a set of classes  $\mathcal{K}$ , we define the OOA of a point cloud segmentation  $\mathcal{S}$  as:

$$l^{\text{oracle}}(S) = \text{mode} \{l_i \mid i \in S\}$$

$$OOA = \frac{1}{|C|} \sum_{S \in \mathcal{S}} \sum_{i \in S} [l_i = l^{\text{oracle}}(S)],$$

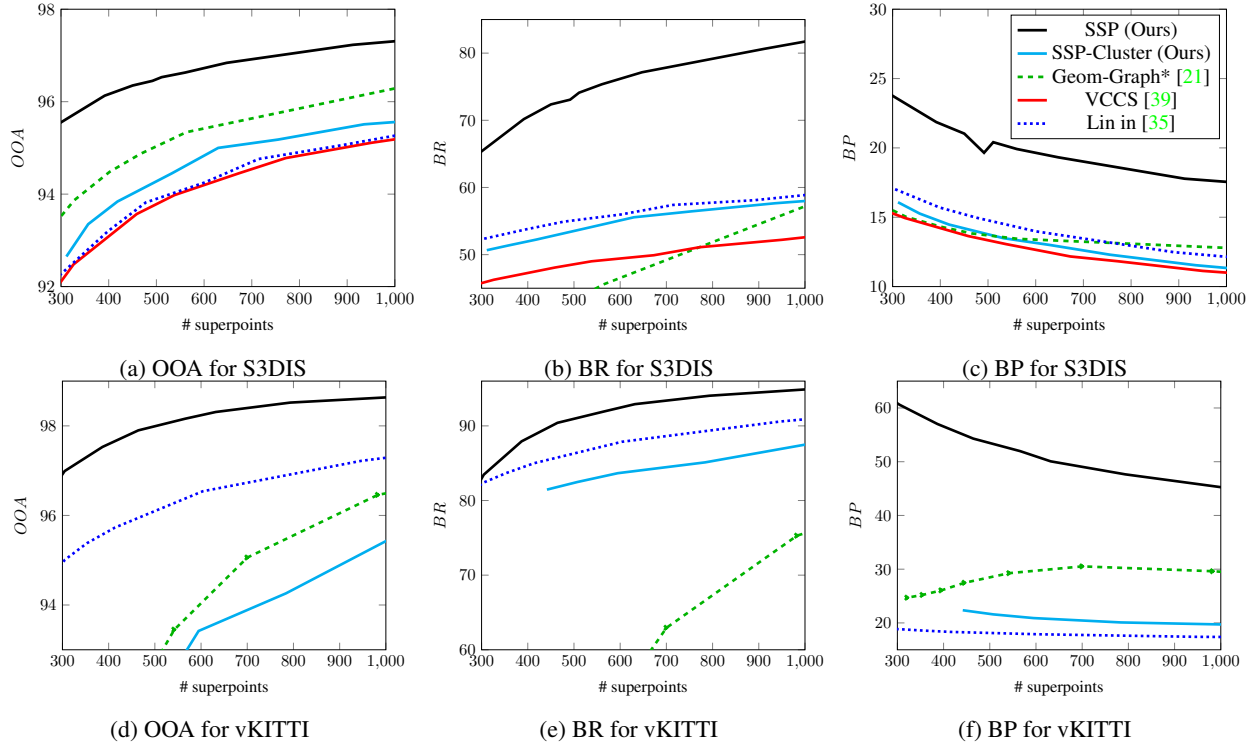


Figure 7: Performance of the different algorithms on the 6-fold S3DIS dataset (a, b, c), and the 6-fold vKITTI dataset (d, e, f). The results of the method annotated with an asterisk \* have not been reported before. SSP-Cluster and VCCS are not represented for vKITTI for the sake of legibility as their performance is too low.

with  $[x = y]$  the function equal to 1 if  $x = y$  and 0 otherwise. Note that the OOA is closely related to the ASA [36], but consider the majority labels of all points within a superpixel rather than the label of the objects with most overlap. In this sense, it is a tighter upper bound to the achievable accuracy of a superpoint-based semantic classification algorithm using  $\mathcal{S}$ . This metric is also more fair than the undersegmentation error [33] for other methods such as [21], or our cluster-based approach, as they do not try to retrieve objects directly, but rather regions of  $C$  with homogeneous semantic labeling.

**Competing algorithms:** We denote by **SSP** (Supervised SuperPoint) our method when using LPE to learn point embeddings and then derive the superpoints using the graph-based methods described in Section 3.2.2, and **SSP-Cluster** when using the cluster-based method defined in Section 3.3 instead. We first assess the benefit of learning embeddings by comparing our results to those of [21], dubbed here **Geom-Graph**. This method computes superpoints by solving the generalized minimal partition problem as well, but with handcrafted geometric features in place of our learned embeddings. We illustrate in Figure 7 the oversegmentations produced by our approach and two state-of-the-art algorithms: **VCCS** [39] and the work of Lin in [35].

We observe that our approach significantly outperforms

the other approaches on all metrics. In particular, we remark that **SSP** only requires under 350 superpoints to reach a performance comparable with **VCCS** with over 1,800 superpoints on S3DIS. Furthermore, the quality of the border is unmatched in our range of superpoints. The improvement is less significant on vKITTI, which could be due to the difficulty of constructing an adjacency graph on such a sparse acquisition. The performance is degraded further without color information, as some transition are not predictable with purely from the geometry. **Geom-Graph** performs well on the accuracy, but not on the boundary. This is expected as the handcrafted geometric features cannot detect some borders, such as adjacent walls. **SSP-Cluster** performs better than the unsupervised cluster-based method of Lin *et al.*, but still suffer from the typical limitations of clustering methods, such as sensitivity to initialization.

In terms of computational speed, the embeddings can be computed very efficiently in parallel on a GPU with over 3 million embeddings per second on a 1080Ti GPU. The bottleneck remains solving the graph partition problem in (9), which can process around 100,000 points per second.

### 4.3. Semantic Segmentation

In Table 1 and Table 2, we show how our point cloud oversegmentation framework can be successfully used by

the superpoint-based semantic segmentation technique of [32]<sup>2</sup> (SPG). We replace the unsupervised superpoint computation with our best-performing approach, SSP. We evaluate the resulting semantic segmentation using standard classification metrics: overall accuracy (OA), mean per-class accuracy (mAcc) and mean per-class intersection-over-union (mIOU). We observe a significant increase in the performance of SPG, beating concurrent methods on both datasets. In particular, we observe that our method allows for better retrieval of small objects (see detailed IoU in the appendix), which translates into much better per-class metrics, although the overall accuracy is not necessarily better than the latest state-of-the-art algorithms.

#### 4.4. Ablation Study

In Table 3, we present an ablation study to empirically justify some of our design choices. To make things more legible, we present the increase/decrease of the 3 performance metrics at 500 superpoints (linearly interpolated) of alternative methods compared to ours, on the first cross-validation fold of the S3DIS dataset. In particular we present **Prop-weight**, an alternative version in which the cross-partition weighting is replaced by a simple inversely-proportional weighting of the inter/intra edges. Predictably, this method gives lesser results as the edges are not weighted according to their influence in the partition. However, since the weights of the intra-edge are proportionally higher, the border precision is improved. We implemented the weights of the segmentation-aware affinity loss of [37] as well for method **SEAL-weights**, with comparable results to the **Prop-weight**. In **+TV-TV**, we replace our choice of function  $\phi$  and  $\psi$  in the loss by respectively  $|\cdot|$  and  $-|\cdot|$ , so that our loss is closer to the pairwise affinity loss used by [12] (but still structured by the graph). However, this approach wouldn't give meaningful partition as the intra-edge term conflicts with the constraint that the embeddings are constrained on the sphere. Removing this restriction leads the collapse of the embeddings around 0. We also tried to stack the LPE in layers, using or not a residual structure comparable to the one used in [22] to increase their receptive fields (more details are given in the appendix). The best results were achieved with two layers: **2-Layers** and **2-Residuals**. However, we observe that when compared with LPE of a similar number of parameters, the gains are insignificant if not null. We conclude that to embed points in order to detect borders, a small receptive field with a shallow architecture is sufficient.

## 5. Conclusion

In this paper, we presented the first supervised 3D point cloud oversegmentation framework. Using a simple point

<sup>2</sup><https://github.com/loicland/superpoint-graph>

Method	OA	mAcc	mIOU
6-fold cross validation			
PointNet [41] in [10]	78.5	66.2	47.6
Engelmann <i>et al.</i> in [10]	81.1	66.4	49.7
PointNet++ [42]	81.0	67.1	54.5
Engelmann <i>et al.</i> in [12]	84.0	67.8	58.3
SPG [32]	85.5	73.0	62.1
PointCNN [34]	<b>88.1</b>	75.6	65.4
SSP + SPG (ours)	87.9	<b>78.3</b>	<b>68.4</b>
Fold 5			
PointNet [41] in [12]	-	49.0	41.1
Engelmann <i>et al.</i> in [12]	84.2	61.8	52.2
pointCNN [34]	85.9	63.9	57.3
SPG [32]	86.4	66.5	58.0
PCCN [54]	-	67.0	58.3
SSP + SPG (ours)	<b>87.9</b>	<b>68.2</b>	<b>61.7</b>

Table 1: Performance of different methods for the semantic segmentation task on the S3DIS dataset. The top table is for the 6-fold cross validation, the bottom table on the fifth fold only.

Method	OA	mAcc	mIOU
PointNet [41]	79.7	47.0	34.4
Engelmann <i>et al.</i> in [12]	79.7	57.6	35.6
Engelmann <i>et al.</i> in [10]	80.6	49.7	36.2
3P-RNN [60]	<b>87.8</b>	54.1	41.6
SSP + SPG (ours)	84.3	<b>67.3</b>	<b>52.0</b>

Table 2: Performance of different methods for the semantic segmentation task on the vKITTI dataset with 6-fold cross validation.

Method	# parameters	OOA	BR	BP
<b>Best</b>	13,816	96.2	73.3	22.1
<b>Prop-weights</b>	13,816	-2.6	-12.2	+10.4
<b>SEAL-weights</b>	13,816	-1.3	-11.3	+3.8
<b>2-Layers</b>	14,688	-0.1	-0.7	-0.3
<b>2-Residuals</b>	14,688	+0.0	-0.2	-0.7

Table 3: Impact of some of our design choice on S3DIS. **Best** is the SSP method with cross-partition weights.

embedding network and a new graph-structured loss function, we were able to achieve significant improvements compared to the state-of-the-art of point cloud oversegmentation. When combined with a superpoint-based semantic segmentation method, our method sets a new state-of-the-art of semantic segmentation as well. A video illustration is accessible at <https://youtu.be/bKxU03tjLJ4>. The source code will be made available to the community as well as trained networks in an update to the superpoint-graph repository<sup>2</sup>. Future work will focus on improving the solving method for the generalized minimum minimal partition problem to better handle spherically-bounded variables, and to improve its computational performance.

## References

- [1] R. Achanta, A. Shaji, K. Smith, A. Lucchi, P. Fua, S. Süsstrunk, et al. Slic superpixels compared to state-of-the-art superpixel methods. *IEEE transactions on Pattern Analysis and Machine Intelligence*, 34(11), 2012. 1, 2, 6
- [2] E. Aljalbout, V. Golkov, Y. Siddiqui, and D. Cremers. Clustering with deep learning: Taxonomy and new methods. *arXiv preprint arXiv:1801.07648*, 2018. 2
- [3] I. Armeni, O. Sener, A. R. Zamir, H. Jiang, I. K. Brilakis, M. Fischer, and S. Savarese. 3d semantic parsing of large-scale indoor spaces. In *CVPR 2016, Las Vegas, NV, USA, June 27-30, 2016*, 2016. 6
- [4] Y. Ben-Shabat, T. Avraham, M. Lindenbaum, and A. Fischer. Graph based over-segmentation methods for 3d point clouds. *Computer Vision and Image Understanding*, 2018. 2
- [5] J. Bromley, I. Guyon, Y. LeCun, E. Säckinger, and R. Shah. Signature verification using a "siamese" time delay neural network. In *Advances in Neural Information Processing Systems*, 1994. 2
- [6] P. Charbonnier, L. Blanc-Féraud, G. Aubert, and M. Barlaud. Deterministic edge-preserving regularization in computed imaging. *IEEE Transactions on Image Processing*, 6(2), 1997. 4
- [7] J. Chen and B. Chen. Architectural modeling from sparsely scanned range data. *International Journal of Computer Vision*, 78(2-3), 2008. 1
- [8] S. Chopra, R. Hadsell, and Y. LeCun. Learning a similarity metric discriminatively, with application to face verification. In *CVPR*, volume 1. IEEE, 2005. 2, 4
- [9] B. Delaunay et al. Sur la sphere vide. *Izv. Akad. Nauk SSSR, Otdelenie Matematicheskii i Estestvennyka Nauk*, 7(793-800):1–2, 1934. 11
- [10] F. Engelmann, T. Kontogianni, A. Hermans, and B. Leibe. Exploring spatial context for 3d semantic segmentation of point clouds. In *ICCV Workshops*, 2017. 2, 6, 8
- [11] F. Engelmann, T. Kontogianni, A. Hermans, and B. Leibe. Exploring spatial context for 3d semantic segmentation of point clouds. In *ICCV, 3DRMS Workshop*, 2017. 12
- [12] F. Engelmann, T. Kontogianni, J. Schult, and B. Leibe. Know what your neighbors do: 3d semantic segmentation of point clouds. In *GMDL Workshop, ECCV*, 2018. 2, 4, 8
- [13] F. Engelmann, T. Kontogianni, J. Schult, and B. Leibe. Know what your neighbors do: 3d semantic segmentation of point clouds. *arXiv preprint arXiv:1810.01151*, 2018. 12
- [14] P. F. Felzenszwalb and D. P. Huttenlocher. Efficient graph-based image segmentation. *International Journal of Computer Vision*, 59(2), 2004. 2
- [15] G. Gao, M. Lauri, J. Zhang, and S. Frintrop. Saliency-guided adaptive seeding for supervoxel segmentation. In *IEEE/RSJ International Conference on Intelligent Robots and Systems, IROS*, 2017. 2
- [16] J. Goldberger, G. E. Hinton, S. T. Roweis, and R. R. Salakhutdinov. Neighbourhood components analysis. In *Advances in Neural Information Processing Systems*, 2005. 2
- [17] G. Gonthier. Formal proof—the four-color theorem. *Notices of the AMS*, 55(11), 2008. 5
- [18] I. Goodfellow, Y. Bengio, A. Courville, and Y. Bengio. *Deep learning*, volume 1. MIT press Cambridge, 2016. 11
- [19] T. Groueix, M. Fisher, V. G. Kim, B. C. Russell, and M. Aubry. Atlasnet: A papier-maché approach to learning 3d surface generation. In *CVPR*. IEEE, 2017. 2
- [20] M. Grundmann, V. Kwatra, M. Han, and I. A. Essa. Efficient hierarchical graph-based video segmentation. In *CVPR*, 2010. 2
- [21] S. Guinard and L. Landrieu. Weakly supervised segmentation-aided classification of urban scenes from 3d lidar point clouds. In *ISPRS Workshop*, 2017. 1, 2, 4, 7
- [22] K. He, X. Zhang, S. Ren, and J. Sun. Deep residual learning for image recognition. In *CVPR*, 2016. 8
- [23] J. R. Hershey, Z. Chen, J. Le Roux, and S. Watanabe. Deep clustering: Discriminative embeddings for segmentation and separation. In *Acoustics, Speech and Signal Processing (ICASSP), 2016 IEEE*. IEEE, 2016. 2
- [24] E. Hoffer and N. Ailon. Deep metric learning using triplet network. In *International Workshop on Similarity-Based Pattern Recognition*. Springer, 2015. 2, 4
- [25] P. J. Huber et al. Robust regression: asymptotics, conjectures and monte carlo. *The Annals of Statistics*, 1(5), 1973. 4
- [26] S. Ioffe and C. Szegedy. Batch normalization: Accelerating deep network training by reducing internal covariate shift. In *ICML*, 2015. 3
- [27] M. Jaderberg, K. Simonyan, A. Zisserman, et al. Spatial transformer networks. In *Advances in Neural Information Processing Systems*, 2015. 3
- [28] V. Jampani, D. Sun, M. Liu, M. Yang, and J. Kautz. Superpixel sampling networks. In *ECCV*, 2018. 1, 2, 5
- [29] D. P. Kingma and J. Ba. Adam: A method for stochastic optimization. *ICLR*, 2015. 11
- [30] B. Kulis et al. Metric learning: A survey. *Foundations and Trends in Machine Learning*, 5(4), 2013. 2
- [31] L. Landrieu and G. Obozinski. Cut pursuit: Fast algorithms to learn piecewise constant functions on general weighted graphs. *SIAM Journal on Imaging Sciences*, 10(4), 2017. 4, 5
- [32] L. Landrieu and M. Simonovsky. Large-scale point cloud semantic segmentation with superpoint graphs. In *CVPR*. IEEE, 2018. 1, 8, 12
- [33] A. Levinshtein, A. Stere, K. N. Kutulakos, D. J. Fleet, S. J. Dickinson, and K. Siddiqui. Turbopixels: Fast superpixels using geometric flows. *IEEE Transactions on Pattern Analysis and Machine Intelligence*, 31(12), 2009. 2, 7
- [34] Y. Li, R. Bu, M. Sun, and B. Chen. PointCNN. *arXiv preprint arXiv:1801.07791*, 2018. 2, 8, 12
- [35] Y. Lin, C. Wang, D. Zhai, W. Li, and J. Li. Toward better boundary preserved supervoxel segmentation for 3d point clouds. *ISPRS Journal of Photogrammetry and Remote Sensing*, 143, 2018. 2, 6, 7
- [36] M.-Y. Liu, O. Tuzel, S. Ramalingam, and R. Chellappa. Entropy rate superpixel segmentation. In *CVPR*. IEEE, 2011. 2, 5, 7
- [37] W.-C. T. M.-Y. Liu, V. J. D. S. Shao-Yi, C. M.-H. Yang, and J. Kautz. Learning superpixels with segmentation-aware affinity loss. In *CVPR*. IEEE, 2018. 1, 2, 5, 8

- [38] V. Nair and G. E. Hinton. Rectified linear units improve restricted boltzmann machines. In *ICML*, 2010. 3
- [39] J. Papon, A. Abramov, M. Schoeler, and F. Wörgötter. Voxel cloud connectivity segmentation - supervoxels for point clouds. In *CVPR*, 2013. 2, 6, 7
- [40] S. Pu, G. Vosselman, et al. Automatic extraction of building features from terrestrial laser scanning. *International Archives of Photogrammetry, Remote Sensing and Spatial Information Sciences*, 36(5), 2006. 1
- [41] C. R. Qi, H. Su, K. Mo, and L. J. Guibas. Pointnet: Deep learning on point sets for 3d classification and segmentation. *CVPR, IEEE*, 1(2), 2017. 1, 2, 3, 8, 12
- [42] C. R. Qi, L. Yi, H. Su, and L. J. Guibas. PointNet++: Deep hierarchical feature learning on point sets in a metric space. In *NIPS*, 2017. 2, 8
- [43] G. Riegler, A. O. Ulusoy, and A. Geiger. OctNet: Learning deep 3D representations at high resolutions. In *CVPR*, 2017. 2
- [44] R. B. Rusu, Z. C. Marton, N. Blodow, M. Dolha, and M. Beetz. Towards 3d point cloud based object maps for household environments. *Robotics and Autonomous Systems*, 56(11), 2008. 1
- [45] R. Salakhutdinov and G. Hinton. Learning a nonlinear embedding by preserving class neighbourhood structure. In *Artificial Intelligence and Statistics*, 2007. 2
- [46] M. Simonovsky and N. Komodakis. Dynamic edge-conditioned filters in convolutional neural networks on graphs. In *CVPR*, 2017. 2
- [47] H. O. Song, S. Jegelka, V. Rathod, and K. Murphy. Learnable structured clustering framework for deep metric learning. *CoRR, abs/1612.01213*, 2016. 2
- [48] S. Song, H. Lee, and S. Jo. Boundary-enhanced supervoxel segmentation for sparse outdoor lidar data. *Electronics Letters*, 50(25), 2014. 2
- [49] D. Stutz, A. Hermans, and B. Leibe. Superpixels: An evaluation of the state-of-the-art. *Computer Vision and Image Understanding*, 166, 2018. 2
- [50] L. P. Tchapmi, C. B. Choy, I. Armeni, J. Gwak, and S. Savarese. SEGCloud: Semantic segmentation of 3D point clouds. *International Conference on 3D Vision*, 2017. 2, 12
- [51] M. Van den Bergh, X. Boix, G. Roig, and L. Van Gool. SEEDS: superpixels extracted via energy-driven sampling. *International Journal of Computer Vision*, 111(3), 2015. 2
- [52] J. Wang, Y. Song, T. Leung, C. Rosenberg, J. Wang, J. Philbin, B. Chen, and Y. Wu. Learning fine-grained image similarity with deep ranking. In *CVPR*, 2014. 3, 4
- [53] J. Wang, F. Zhou, S. Wen, X. Liu, and Y. Lin. Deep metric learning with angular loss. In *ICCV. IEEE*, 2017. 2
- [54] S. Wang, S. Suo, W.-C. M. A. Pokrovsky, and R. Urtasun. Deep parametric continuous convolutional neural networks. In *CVPR*, 2018. 2, 8
- [55] Y. Wu and K. He. Group normalization. *ECCV*, 2018. 11
- [56] X. Xiong, D. Munoz, J. A. Bagnell, and M. Hebert. 3-d scene analysis via sequenced predictions over points and regions. In *ICRA IEEE. IEEE*, 2011. 1
- [57] C. Xu and J. J. Corso. Evaluation of super-voxel methods for early video processing. In *CVPR*, 2012. 2
- [58] J. Yao, M. Boben, S. Fidler, and R. Urtasun. Real-time coarse-to-fine topologically preserving segmentation. In *CVPR*, 2015. 2
- [59] X. Ye, J. Li, H. Huang, L. Du, and X. Zhang. 3D recurrent neural networks with context fusion for point cloud semantic segmentation. In *ECCV. Springer*, 2018. 2
- [60] X. Ye, J. Li, H. Huang, L. Du, and X. Zhang. 3d recurrent neural networks with context fusion for point cloud semantic segmentation. In *ECCV*, 2018. 8
- [61] T. Zhang et al. Some sharp performance bounds for least squares regression with l1 regularization. *The Annals of Statistics*, 37(5A), 2009. 4
- [62] Y. Zhou and O. Tuzel. Voxelnet: End-to-end learning for point cloud based 3d object detection. In *CVPR*, 2017. 2

## Supplementary Material

### A. Models configuration

In this section, we give the full hyper-parameterization of all the networks used in the paper, for both oversegmentation and semantic segmentation tasks, and for both datasets.

#### A.1. Models configuration for oversegmentation

Our supervised oversegmentation model has a number of critical hyper-parameters to tune, given in Table 4. We detail here the rationale behind our choices.

**Local neighborhood and adjacency graphs:** For both datasets, we find that setting the local neighborhood size to 20 was enough for embeddings to successfully detect objects’ border. Combined with our lightweight structure, this results in a very low memory load overall. The adjacency graph  $G$  requires more attention depending on the dataset. For the dense scans of S3DIS, the 5-nearest neighbors adjacency structure was enough to capture the connectivity of the input clouds. For the sparse scans of vKITTI, we added Delaunay edges [9] (pruned at 50 cm) such that parallel scans lines would be connected.

**Networks configuration:** For the LPE and the PointNet structure in the spatial transform, we find that shallow and wide architectures works better than deeper networks. We give in Table 4 the size of the linear layers, before and after the maxpool operation. Over 250,000 points can be embedded simultaneously on 11GB RAM in the training step, while keeping track of gradients.

**Intra-edge factor:** The graph-structured contrastive loss presented in 3.2.2 requires setting a weight  $\mu$  determining the influence of inter-edges with respect to intra-edge. Since most edges of  $G$  are intra-edges in practice, we define  $\tilde{\mu}$  such that  $\mu = \tilde{\mu}c$  with  $c = |E|/|V|$  the average connectivity of  $G$ . Note that  $c$  can be determined directly from the construction of the adjacency graph (it is equal to  $k$  in a  $k$ -nearest neighbor graph for example). A value of  $\tilde{\mu} = 1$  means that the total influence in  $\ell$  of inter-edges and intra-edges are identical. Since we are interested in oversegmentation, we set  $\tilde{\mu}$  to 5 in all our experiments, but note that the network is not very sensitive to this parameter, as demonstrated experimentally: a value of  $\tilde{\mu} = 3$  gives a relative performance of  $(-0.2, -0.6, +1.5)$  while a value of 8 gives  $(+0.1, -0.5, +1.4)$ .

**Regularization Strength:** The generalized minimal partition problem defined in 3.2.1 requires setting the regularization strength factor  $\lambda$ , determining the cost of edges crossing superpoints. We remark that the LPE produces embeddings of points with an euclidean distance of at least 1 over predicted objects’ borders. Some calculus shows us that for a  $\lambda \leq 1/(2c)$ , the solution  $f^*$  of (8) should predict superpoints borders at all edges whose vertices have a difference of embeddings of at least 1 (note that there is no guarantee that the greedy  $\ell_0$ -cut pursuit algorithm will indeed predict a border). We use this value to define a normalized regularization strength  $\tilde{\lambda}$  such that  $\lambda = \tilde{\lambda}/(4c)$ , whose default value is 1.

**Regularization path:** To obtain the regularization paths in Figure 7, we first train the network with a regularization strength of  $\tilde{\lambda} = 1$  (see 3.2.2). We then compute partitions with  $\tilde{\lambda}$  varying from 0.2 to 6 with no fine-tuning required.

**Smallest superpoint:** To automatically select a minimal superpoint size (in number of points) appropriate to the coarseness of the segmentation, we heuristically set:

$$n_{\min}^{\tilde{\lambda}} = \left[ \left( \max \left( \frac{1}{2}n_{\min}^{(1)}, n_{\min}^{(1)} + \frac{1}{2}n_{\min}^{(1)} \log(\tilde{\lambda}) \right) \right) \right]$$

where  $n_{\min}^{(1)}$  is a dataset-specific minimum superpoints size for  $\tilde{\lambda} = 1$ . For example, for  $n_{\min}^{(1)} = 50$ , the smallest superpoint allowed for a small regularization strength  $\tilde{\lambda} = 0.2$  will be 33, while it is 70 for the coarse partition obtained with  $\tilde{\lambda} = 6$ . While specific applications may require setting up this variable manually, this allowed us to produce the regularization paths in Figure 7 while only varying  $\tilde{\lambda}$ .

**Optimization:** Given the small size of our network, we train our network for a short number of epochs (see Table 4), with decay events set at 0.7. We use Adam optimizer [29] with gradient clipping at 1 [18]. Training takes around 2 hours per fold on our 11GB VRAM 1080Ti GPU.

**Mini-batches:** For graph-based clustering, the training phase processes batches of 16 point clouds at once, for which a subgraph of size 10 000 points is extracted. For the clustering-based segmentation, which is more memory intensive, and since subgraphs have to be larger to be meaningfully covered by the initial voxels, we set a batch size of 1 and a subgraph of 100 000. As a consequence, we replace the batchnorm layers of the LPEs by group norms with 4 groups [55].

**Augmentation:** In order to build more robust networks, we added Gaussian noise of deviation 0.03 clamped at 0.1 on the normalized position and color of neighborhood clouds. We also added random rotation of the input clouds for the network to learn rotation invariance. To preserve orientation information, the clouds are rotated as a whole instead of each neighborhood. This allows the spatial transform to detect change in orientation, which can be used to detect borders.

#### A.2. Models configuration for semantic segmentation

We used the open-source superpoint-graph implementation [github/loicland/superpoint-graph](https://github.com/loicland/superpoint-graph) without any modification beyond changing the oversegmentation step and some changes in the hyper-parameters. The full parameterization is given in Table 5.

To compensate for the edges missed by the  $\ell_0$ -cut pursuit approximation, due in part to its ignoring the spherical nature of the embeddings, we set the regularization strength  $\tilde{\lambda}$  lower than 1 for both datasets. This help improve the accuracy and border recall. The subsequent decrease in border precision is compensated by the fact that the SPG, through its context leveraging module, can learn to propagate the semantic information to small superpoints.

parameter	shorthand	section	S3DIS	vKITTI
Local neighborhood size	$k$	3.1		20
# parameters	-	-		13,816
LPE configuration	-	3.1	[32,128],[64,32,32,m]	
ST configuration	-	3.1	[16,64],[32,16,4]	
Embeddings dimension	$m$	3.1		4
Adjacency graph	$G$	3.2	5-nn	5-nn + Delaunay
exponential edge factor	$\sigma$	3.2.1		0.5
intra-edge factor	$\tilde{\mu}$	3.2.3		5
spatial influence	$\alpha^{\text{spatial}}$	3.4	0.2	0.02
smallest superpoint	$n_{\min}^{(1)}$	3.4	40	10
epochs	-	-		50
decay event	-	-		20,35,45

Table 4: Configuration of the embedding network for the S3DIS and vKITTI datasets.

parameter	S3DIS	vKITTI
# parameters	278,897	118,737
Superpoint embedders configuration	[[64,64,128,128,256], [256,64,32]]	[[64,64,128,256], [128,32,32]]
STN configuration	[[64,64,128], [128,64]]	[[32,32,64], [64,32]]
subsampling hops		4
max SPgraph size		768
$\lambda$	0.1	0.5
$n_{\min}$	25	15
epochs	350	100
decay event	180,250,280,320	40,50,60,70,80

Table 5: Configuration of the semantic segmentation network. All values not mentioned in this table use default parameters from [32]

Method	OA	mAcc	mIoU	ceiling	floor	wall	beam	column	window	door	chair	table	bookcase	sofa	board	clutter
A5 PointNet [41]	-	49.0	41.1	88.8	97.3	69.8	<b>0.1</b>	3.9	46.3	10.8	52.6	58.9	40.3	5.9	26.4	33.2
A5 SEGCloud [50]	-	57.4	48.9	90.1	96.1	69.9	0.0	18.4	38.4	23.1	75.9	70.4	58.4	40.9	13.0	41.6
A5 PointCNN [34]	85.9	63.9	57.3	<b>92.3</b>	<b>98.2</b>	79.4	0.0	17.6	22.8	62.1	80.6	74.4	66.7	31.7	<b>62.2</b>	<b>56.7</b>
A5 SPG [32]	86.4	66.5	58.0	89.4	96.9	78.1	0.0	<b>42.8</b>	48.9	<b>61.6</b>	84.7	75.4	69.8	<b>52.6</b>	2.1	52.2
A5 SSP + SPG (ours)	<b>87.9</b>	<b>68.2</b>	<b>61.7</b>	91.9	96.7	<b>80.8</b>	<b>0.0</b>	28.8	<b>60.3</b>	<b>57.2</b>	<b>85.5</b>	<b>76.4</b>	<b>70.5</b>	49.1	51.6	53.3
PointNet [41] in [11]	78.5	66.2	47.6	88.0	88.7	69.3	42.4	23.1	47.5	51.6	42.0	54.1	38.2	9.6	29.4	35.2
Engelmann <i>et al.</i> [11]	81.1	66.4	49.7	90.3	92.1	67.9	44.7	24.2	52.3	51.2	47.4	58.1	39.0	6.9	30.0	41.9
Engelmann in [13]	84.0	67.8	58.3	92.1	90.4	78.5	37.8	35.7	51.2	65.4	61.6	64.0	51.6	25.6	49.9	53.7
SPG [32]	85.5	73.0	62.1	89.9	95.1	76.4	62.8	47.1	55.3	68.4	73.5	69.2	63.2	45.9	8.7	52.9
PointCNN [34]	<b>88.1</b>	75.6	65.4	<b>94.8</b>	<b>97.3</b>	75.8	<b>63.3</b>	51.7	58.4	57.2	69.1	<b>71.6</b>	61.2	39.1	52.2	58.6
SSP + SPG (ours)	87.9	<b>78.3</b>	<b>68.4</b>	91.7	95.5	<b>80.8</b>	62.2	<b>54.9</b>	<b>58.8</b>	<b>68.4</b>	<b>78.4</b>	69.2	<b>64.3</b>	<b>52.0</b>	<b>54.2</b>	<b>59.2</b>

Table 6: Results on the S3DIS dataset on fold “Area 5” (top) and micro-averaged over all 6 folds (bottom). Intersection over union is shown split per class, with the highest value over all methods in bold.

For the same reason, we chose a lower superpoint size for S3DIS from the segmentation experiments.

We extended the superpoint graph subsampling threshold to 4-hops instead of 3, because our method SSP tends to produce thin components near interfaces. Since the vKITTI dataset is much smaller than S3DIS, we chose smaller networks to mitigate overfitting.

## B. Residual Point Embedder

We have tested an alternative configuration for the local point embedded, in which they were stacked in layers, similarly to the classical convolutional architecture for images. We first introduce a slightly changed architecture, the Residual Point Embedder RPE, whose design is based on an LPE but takes a supplementary input

$e_{\text{ini}}$ . Instead of computing a new embedding, the RPE computes a residual (10) which is added to this initial embedding before normalization (11):

$$R(X_i, x_i) = \text{MLP}_2([\max(\text{MLP}_1(X_i)), x_i]) \quad (10)$$

$$\text{RPE}(x_i, X_i, e_{\text{ini}}) = \text{L}_2(e_{\text{ini}} + R(X_i, x_i)) \quad (11)$$

The second change is the layers architecture. The RPEs in the first layer compute the embeddings from the local geometric and radiometric information alone, and their initial embedding is set to 0 (12) (such that they behave exactly like LPEs). The RPEs in subsequent layers compute new embeddings from the local radiometry and geometry as well as the embeddings computed at the previous layer of the points neighbors  $E_i^t$  (13). Note that for a point to be processed by a layer, all its neighbors must have been embedded by the previous layer. This allows the RPEs to have increasingly broader receptive fields, and to correct errors that might have been done by previous layers. Note that the geometric information are

only processed by the spatial transform once, cascading its values to all residual layers.

$$e_i^{(0)} = \text{RPE}^{(0)}([\tilde{P}_i, R_i], [\tilde{p}_i, r_i], 0) \quad (12)$$

$$e_i^{(t+1)} = \text{RPE}^{(t)}([\tilde{P}_i, E_i^{(t)}], [\tilde{p}_i, r_i, e_i^{(t)}], e_i^{(t)}) \quad (13)$$

Alternatively, all initial embeddings can be set to 0, which means that each layer computes a new embedding from the local position and the embeddings of the previous layers. As mentioned in the ablation study, while these networks did perform well, their benefits shrink when a simple LPE is given as many parameters.

## C. Detailed results and illustration

We present in Table 6 the per-class IoU for the S3DIS dataset. We illustrate the semantic segmentation results in Figure 8. We also made a video illustration which can be accessed at <https://youtu.be/bKxU03tjLJ4>.

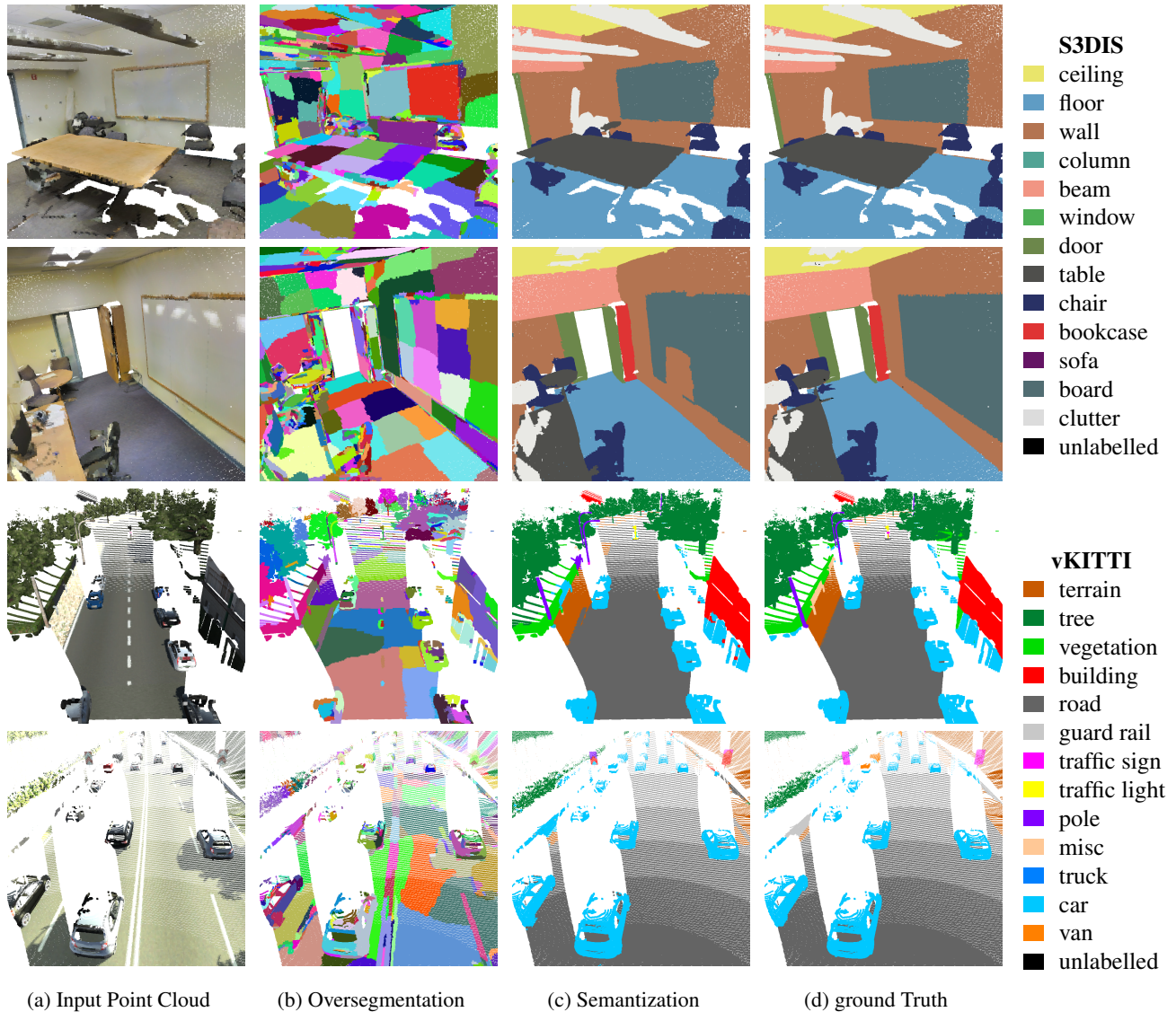


Figure 8: Illustration of the results on the semantic segmentation. In the first row we show a successful semantization for a complex scene of S3DIS. In the second row, we show a failure case in which a white board is oversegmented in too many small superpoints. This makes their classification harder by the semantic segmentation network. In the third row we see a successful semantization of an urban outdoor scene from vKITTI. On the fourth row, we can observe in the background road signs with high color contrasts, which are segmented in small superpoints. This makes them very hard to classify and they are missed by the semantic segmentation algorithm.